Journal of Biomedical Optics

SPIEDigitalLibrary.org/jbo

Integrated ultrasound and photoacoustic probe for co-registered intravascular imaging

Wei Wei
Xiang Li
Qifa Zhou
K. Kirk Shung
Zhongping Chen

SPIE

Integrated ultrasound and photoacoustic probe for co-registered intravascular imaging

Wei Wei,[a,b,*] Xiang Li,[c,*] Qifa Zhou,[c] K. Kirk Shung,[c] and Zhongping Chen[b]
[a]Wuhan University, Department of Physics and Key Laboratory of Acoustic and Photonic Materials and Devices, Ministry of Education, Wuhan 430072, China
[b]University of California, Irvine, Beckman Laser Institute and Medical Clinic, Department of Biomedical Engineering, Irvine, California 92612–1475
[c]University of Southern California, NIH Transducer Resource Center and Department of Biomedical Engineering, California 90089

Abstract. We report on the synergy of an integrated ultrasound (US) and photoacoustic (PA) probe system for intravascular imaging. The combined dual-modality probe is based on a 39 MHz ring-shaped US transducer which detects both US echoes and laser-generated PA signals. By combining optical fiber, US transducer, and micromirror, we can obtain intravascular cross-sectional B-scan images by internal illumination of the sample. The performance of the probe is evaluated in a phantom study. Moreover, the coaxially designed probe also provides co-registered US and PA images of a normal rabbit aorta, which demonstrates the imaging ability of the dual-functional system, implying future clinical applications. [DOI: 10.1117/1.3631798]

Keywords: ultrasound; photoacoustic imaging; endoscopic imaging.

Paper 11156RR received Mar. 28, 2011; revised manuscript received Aug. 7, 2011; accepted for publication Aug. 9, 2011; published online Oct. 3, 2011.

1 Introduction

Atherosclerosis is a complex disease in which multiple plaques build up within the arteries. In the course of time, the plaque hardens and narrows the artery. As a result, it causes many related diseases, such as coronary heart disease, carotid artery disease, and peripheral arterial disease, and, as such, is one of the major causes of morbidity and mortality in developed countries.[1] Currently, several biomedical imaging techniques aimed at imaging and assessing vulnerable plaques have been reported in the literature, such as angiography, magnetic resonance imaging (MRI), electron-beam computed tomography (EBCT), optical coherence tomography (OCT), and intravascular ultrasound (IVUS).[2–6] However, all of them have limitations. Angioscopy allows the plaque to be visualized with high sensitivity, but the morphologic characterization of the plaque is unreliable because of the lack of estimation of cap thickness or lipid content.[2] MRI is performed to study the progression and regression of plaque over time, however, its insufficient resolution cannot render accurate measurements.[2] EBCT specifically predicts plaque calcium; however, it has limited identification for physiologic significance and vulnerability of plaque (i.e., obstructive or nonobstructive, stable or unstable).[3] Although OCT has been used for vulnerable plaque evaluation and it is able to measure microscopic features with its high resolution, it cannot image the whole depth of a large lipid pool of a plaque due to limited penetration depth.[2,4–6] IVUS has proved to be capable of visualizing the structural information of the artery wall with large penetration depth and its moderate resolution can resolve plaque, lipid pool, and vessel structures; however, the image contrast might be insufficient to distinguish complex constituents.[2,5,6]

PA imaging has been newly developed as a hybrid imaging technique for its safety and high ratio of imaging depth to resolution.[7–11] The PA signal resulting from the electromagnetic wave absorption of tissues can be collected and spatially resolved by an US transducer. Once the transient acoustic wave is excited, it can provide the mapping of optical absorption distribution of tissue constituents. In recent publications, Emelianov's group reported that intravascular photoacoustic (IVPA) imaging succeeded in identifying the different constituents of fibrocellular inflammatory plaque.[12,13] However, the external light illumination design is not feasible for *in vivo* experiments. For typical IVUS applications, a miniaturized ultrasound probe is attached to the distal end of a specially designed catheter, which allows the doctor to acquire images from the inside of a vessel. Therefore, the integration of an IVPA probe with an IVUS catheter has been developed as an essential modality for detecting and identifying ruptured plaques.[14–18]

In this paper, we present a successfully integrated US and PA probe employing illumination optics in a ring-shaped US transducer. The optical fiber was inserted through the central hole of the ring transducer, forming a coaxial design, which is essential in providing co-registered images. The spatial resolution of the probe was investigated by imaging tungsten wires. We carried out a tissue-mimicking phantom study to analyze the performance of the probe. Moreover, a real tissue experiment was conducted to show the imaging ability of the probe.

[*]These authors contributed equally to this work.

Address all correspondence to: Zhongping Chen, E-mail: z2chen@uci.edu; Qifa Zhou, E-mail: qifazhou@usc.edu.

1083-3668/2011/16(10)/106001/6/$25.00 © 2011 SPIE

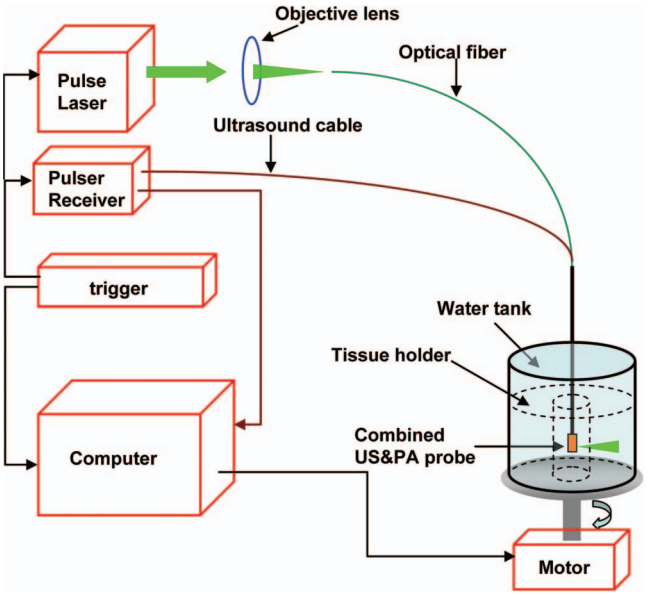

Fig. 1 Prototype of the hybrid IVUS and IVPA imaging systems.

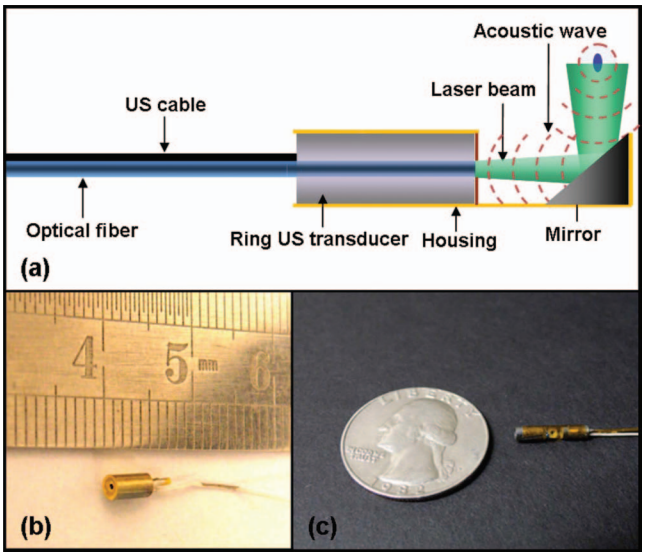

Fig. 2 (a) Schematic of the combined US and PA probe. (b) Photo of the hand-crafted ring-shaped US transducer. (c) Photo of the combined US and PA probe after packaging.

2 Materials and Methods

2.1 *US-Based Integrated Imaging System*

In our US-based integrated imaging system (Fig. 1), we used the pulsed Q-switched Nd:YAG laser (532 nm wavelength, 3 to 5 ns pulse width, 10 Hz repetition rate; Continuum, Inc., Santa Clara, California) as the PA signal excitation source. The free space laser output was focused by an objective lens and coupled into an optical fiber for delivery. The light delivery system was combined with a 39 MHz ring-shaped US transducer, which was developed in our laboratory. The combined probe was inserted into the lumen of a sample and the target area was illuminated internally at a surface fluence of 13 mJ/cm^2. The energy is under the American National Standards Institute safety limit of 20 mJ/cm^2.[19] The sample was immersed and fixed in a water tank. The circumferential scanning (B-scan) was accomplished by rotating the tank which was driven by a stepping motor. The pulser and receiver unit (PR5900; Olympus NDT, Inc., Kennewick, Washington) was used to generate US pulses and receive both US echoes and PA waves. For each circular B-scan, 1000 time-resolved PA signals (A-lines) and 1000 US echoes were recorded. The received US echoes and PA signals were amplified by 36 dB through the preamplifier (MITEQ AU-1466; MITEQ Inc., Hauppauge, New York), and then digitized by a 14-bit data acquisition board (Gage Applied Technologies, Lockport, Illinois) with a sampling rate of 200 MHz. A digital bandpass filter (15 to 60 MHz) was applied to the signal to minimize the noise. Signal averaging was used to improve the signal-to-noise ratio. The noise level was quantified to be 0 dB. Relative to the noise level, the maximum acoustic signal amplitude was quantified to be 50 dB in the IVUS image and 40 dB in the IVPA image.

2.2 *Integrated US and PA Probes*

Normally, the probe is designed by mounting the polished fiber tip and US transducer either side by side or mounting the transducer in front of the fiber tip.[17,18] Based on this geometry, the overlap portion of the laser beam and ultrasound beam is determined by the face angle of the polished fiber and the distance between the fiber tip and the transducer. In this case, the working distance of the probe is finite (e.g., 0.5 to 4.5 mm in Jansen's design).[18] However, if the vessel size is larger than this working distance, parts of the vessel would not be covered in one circumferential B-scan.[20,21] The uncovered area would increase when the probe is not positioned at the center of the vessel lumen. Additionally, in order to get highly efficient acoustic signals, the multiple components need to be precisely aligned. In this paper, we present a coaxial integrated probe design, which can ease the requirement of precise alignment and potentially improve the probe's working distance.

Figure 2(a) shows the schematic of our integrated US and PA probe. The 532 nm pulse laser beams were delivered by a 200-μm core multimode optical fiber and emitted through the central hollow of the ring-shaped US transducer. Our design steered both the coaxial laser beams and the US beams into the sample by a customized microrod mirror (platinum coating, 2.0 mm diam, 4 mm length, with the reflective surface angled at 45 deg to the probe's axis). Also, the US echoes and the excited PA waves from the sample were deflected by the mirror and detected by the US transducer. The microrod mirror shared by the coaxial laser and acoustic beam makes alignment of the US transducer and optical probe more precise and robust. Moreover, this design guaranteed that the laser beam and acoustic beam overlapped along the whole transmitting path. Snell's law governs the path of reflected and refracted waves when the acoustic wave encounters an interface of two media.[22] In our experiment, the ratio of sound-propagation speeds (1.5/5.1, longitudinal wave; 1.5/3.3, shear wave) in water and glass was large enough so that the total internal reflection occurred at the interface of water and glass.[11] In other words, there was no additional propagation loss on the transmitting path of the ultrasonic wave. The mirror, optical fiber, and US transducer were fixed and packaged in a polyimide tube in which a window was made to allow the laser beam and US beam to pass through. Figure 2(b) shows the

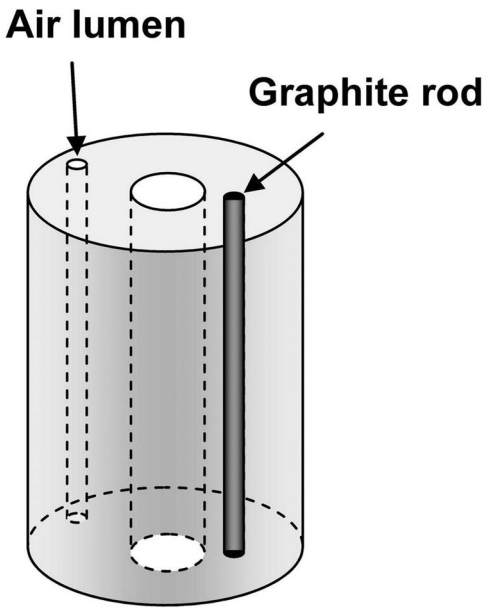

Fig. 3 Three-dimensional schematic of the phantom in which the 0.5 mm diameter graphite rod and 0.5 mm diameter air lumen are embedded. The graphite rod and air lumen work as two contrast inclusions which have a different absorption coefficient within a tissue-mimicking phantom.

ring-shaped US transducer with 2.2 mm outer diameter and 0.6 mm inner diameter. Figure 2(c) is the whole integrated probe that was packaged in a polyimide tube with a final packaged diameter of 2.3 mm. Yang presented a photoacoustic endoscopy using a comparable design,[11] but the probe size is 4.2 mm in diameter, which makes it possible for endoscopic, but not intravascular, imaging. The probe we developed is about half its size in diameter, and it is feasible for IVPA imaging. The size reduction in the intravascular probe represents a significant technical advance in IVPA imaging.

2.3 *Tissue-Mimicking Phantom and Rabbit Aorta Sample*

In order to test the performance of the probe, we needed to first conduct a tissue-mimicking phantom study to obtain IVUS and IVPA images. The cylindrical phantom was made out of 10 wt.% gelatin. Then, 2 wt.% 0.5 to 15 μm silica dioxide powder and 10 vol.% low-fat milk were added as ultrasonic scatterers and optical scatterers, respectively. As shown in Fig. 3, a 5 mm diameter hollow was drilled in the center of the phantom and acted as the lumen of tissue. A 0.5 mm diameter graphite rod, serving as the optical absorption contrast, was embedded in the phantom at a distance of 3.5 mm from the center. By drilling the phantom, we created a 0.5 mm diameter air lumen, the same dimension as the graphite rod, which appeared as an air bubble in the cross-section scanned. The tiny air lumen was 5 mm away from the center and acted as the acoustic contrast.

In order to demonstrate the imaging ability of this dual-modality system, we prepared a section of normal rabbit aorta. For fixation, the aorta (only vascular) was immersed in 10% formalin for 24 h and then preserved in phosphate buffer. The aorta was pinned to a piece of cork and immersed in saline during the experiment.

3 Result and Discussion

3.1 *Resolution of the Combined System*

The resolution of the combined IVUS/IVPA was determined by the US transducer since the laser beam was not focused. The US transducer had a center frequency of 39 MHz and fractional bandwidth of 74%. In order to determine the resolution of the system, we performed PA image tests of five 20 μm diameter tungsten wires in water. The resolution of the IVUS subsystem was proven to be consistent with the theoretical value for a ring transducer with mirror[23] so we focused on the spatial resolution of the IVPA subsystem. Figure 4(a) shows the linear B-scan image of five 20 μm diameter tungsten wires in water. We acquired A-line signals from the tungsten wires. After Hilbert transform processing, we determined the PA axial and lateral resolutions from the -6 dB envelope width. In Fig. 4(b), the axial resolution slowly degrades from 34 to 40 μm, while the target distance is moving from 1.25 to 3.85 mm from the probe. As shown in Fig. 4(c), the lateral resolution changes from 230 to 480 μm as the distance between the probe and wire increases.

3.2 *Tissue-Mimicking Phantom Images*

The images of a tissue-mimicking phantom from the same cross-section were obtained by the combined IVUS and IVPA system. All images in Fig. 5 cover a 13 mm diameter field of view. Figure 5(a) is the IVUS image showing the general structure of the phantom, the lumen, and two inclusions. The 8 o'clock inclusion had a strong signal at a depth of ~2.5 mm and that of the 1 o'clock inclusion had a strong signal at a depth of ~1.0 mm. As prepared previously, we knew one was the graphite rod while the other one was the air lumen. These two inclusions had relatively distinct acoustic impedance compared to the surrounding tissues so both of them appeared as hyperechoic regions. Besides being located at different depths, it was difficult to distinguish the two inclusions from each other by looking at the pattern of the IVUS image. In this case, IVPA, which has the ability to show the optical specificity and the contrast within a phantom tissue, was required. The IVPA image shown in Fig. 5(b) demonstrates an optical absorption contrast within the phantom. According to the PA imaging mechanism, the bright area in Fig. 5(b) implies an optical inclusion which has high absorption at the 532 nm wavelength while the other tissue predominantly scatters the light. Figure 5(c) is the combined image of the phantom. Compared to the surrounding tissue and the air lumen, the absorption of the graphite rod is higher at wavelength 532 nm. Hence, the reflective area located at the 1 o'clock position in Fig. 5 should be the graphite rod, which matches the depth illustration in Fig. 3. On the other hand, we can deduce that the 8 o'clock position in the image is the air lumen by comparing the IVUS and IVPA images. Therefore, by combining these two imaging systems together, the whole tissue structure can be displayed while the relative area of the inclusion can be recognized. The complementary information from the images of the IVUS and IVPA illustrate the synergy of the combined system.

3.3 *Normal Rabbit Aorta Images*

By using the dual-modality probe, *in vitro* images of a normal rabbit aorta were obtained to demonstrate imaging ability. It is

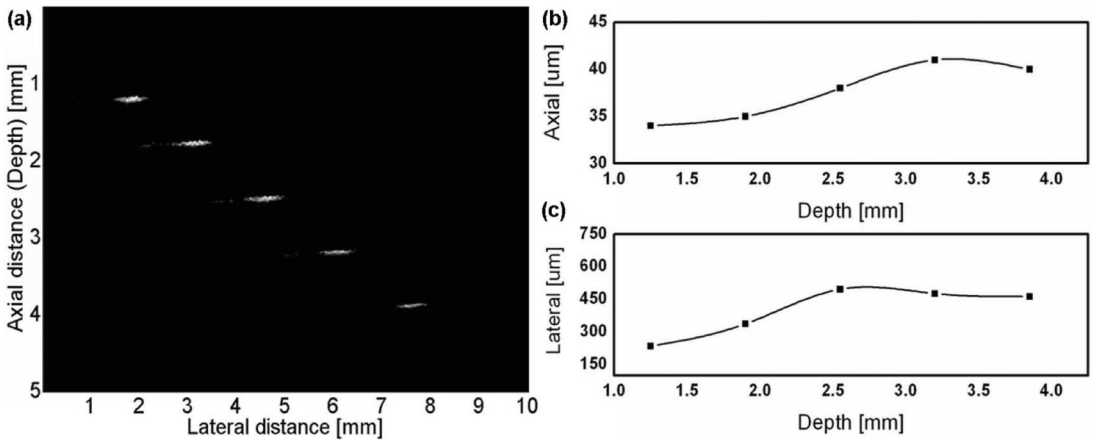

Fig. 4 (a) PA image of five 20 μm tungsten wires. (b) and (c) Axial and lateral resolution versus target distance.

clear that the IVUS image, shown in Fig. 6(a), provides a full-depth cross-sectional image of the aorta. The US pulse echo signals are relatively homogeneous from the vessel wall. Figure 6(b) is the IVPA image from the same cross-section of the aorta. The aorta vessel wall is composed of three layers (Intima, Media, and Adventitia) and tissue in each layer absorbs the light, but with different absorption coefficients (e.g., 10.04 cm^{-1} for Intima, 5.32 cm^{-1} for Media, and 13.29 cm^{-1} for Adventitia at 532 nm).[24] The moderate response from the aorta implies the tissue absorption at 532 nm is sufficient to get an image. The PA signal intensity is also relatively homogeneous, which corresponds well to the IVUS image. At the 6 o'clock position in Fig. 6(b), the IVPA image shows a maximum imaging depth of approximately 1 mm. Figure 6(c) is the hematoxylin and eosin (H&E) stained normal rabbit aorta histological image. As you can see in Fig. 6(c), the vessel wall has a relatively uniform composition at the same cross-section, so it is reasonable that the IVUS and the IVPA images do not indicate any obvious layered structure or special signal appearance in the IVUS and IVPA images. Figure 6(d) shows the combined IVUS–IVPA image. The similar shapes of US and PA images indicate the superiority of the coaxial probe design in obtaining coregistered images.

3.4 *Discussion*

Currently, the diameter of the integrated probe is 2.3 mm after packaging. The reduction in probe size is essential to translate this technology for intravascular imaging. The ring-shaped US transducer could be miniaturized so that the size of the probe implemented can be further reduced. This will benefit the imaging of smaller vessels, such as coronary arteries. By focusing the ring-shaped US transducer, the lateral resolution can be greatly improved for both IVUS and IVPA imaging.[23] As a result, it would provide more detailed information on the vessel structures. The wavelength we used for the phantom study and *in vitro* experiment was 532 nm. For *in vivo* experiments and clinical applications, the blood interference needs to be considered. For example, even though the absorption coefficients of artery vessel and plaque constituents are very different at a wavelength of around 500 to 600 nm, hemoglobin and oxyhemoglobin have even higher optical absorption rates that can obscure artery tissue and plaque constituents at this wavelength range.[24] In this case, the blood left in the vessel will absorb most of the light at these wavelengths and feed back strong PA responses. As a result, the image of the artery wall structure and plaque would be hard to recognize. Flushing and balloon occlusion are standard techniques to reduce the blood

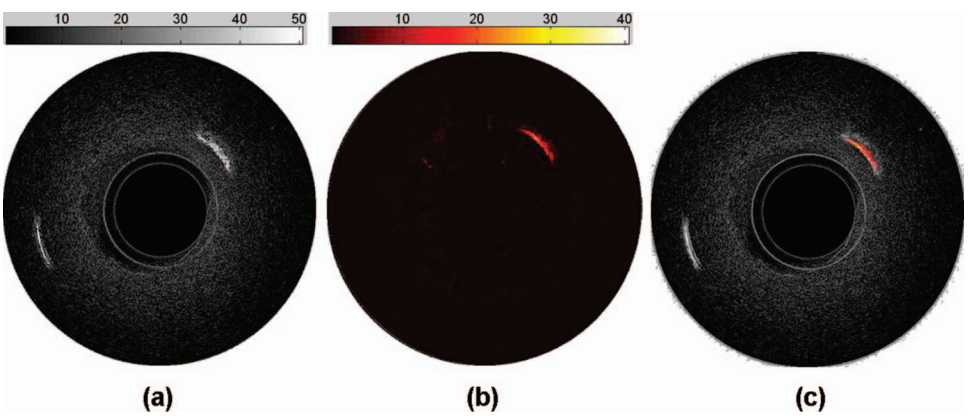

Fig. 5 Cross-sectional (a) IVUS, (b) IVPA, and (c) combined image of the phantom. The field of view is 6.5 mm in radius in all images. IVUS and IVPA images are displayed in dynamic ranges of 50 and 40 dB.

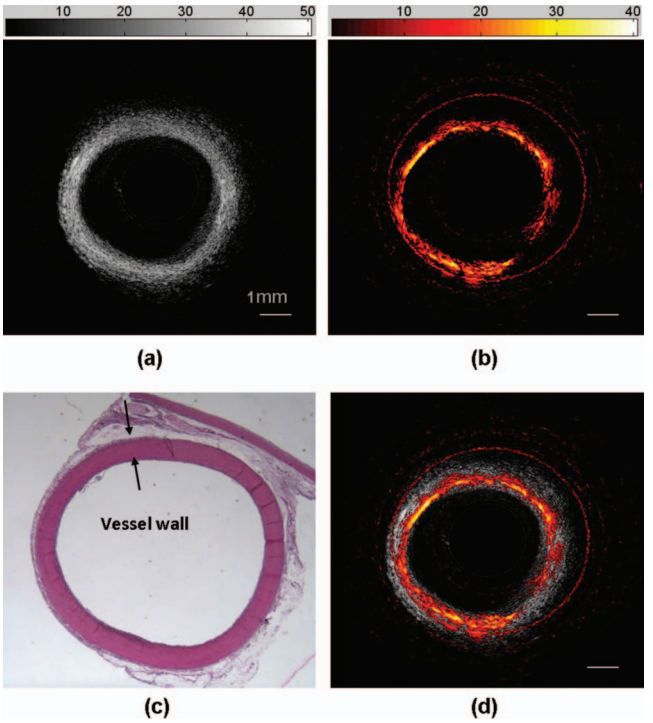

Fig. 6 Cross-sectional (a) IVUS, (b) IVPA, (c) H&E stained histology image, and (d) combined image of a normal rabbit aorta. The IVPA image was obtained using 532 nm optical excitation wavelength and 39 MHz ring-shaped transducer. IVUS and IVPA images are displayed in dynamic ranges of 50 and 40 dB.

interference for intravascular OCT imaging which can be adapted for IVPA imaging.[25] Although the exciting wavelength of 532 nm provides a limited contrast for lipid structures, there are extrinsic contrasts, such as targeted nanoparticles, that can be excited by this wavelength. These extrinsic IVPA contrasts may be used for studying vascular diseases.[26] Lipid contrast is an exciting new development in diseased vessel diagnosis by IVPA. In recent publications,[13,18,27–29] near-infrared (NIR) wavelengths have been proven to be feasible to image diseased vessels and also enhance the lipid contrast. The probe demonstrated in this paper can be used for multispectral intravascular photoacoustic imaging using NIR wavelength excitation. However, our focus was on the demonstration of a small intravascular probe based on a ring transducer, which is a novel advance in IVPA probe development. By introducing the coaxial light delivery system to the ring-shaped US probe, we succeeded in irradiating the sample internally from our combined prototype system. Incorporation of a micromotor[11] or a rotational joint[30] in the probe will enable *in vivo* intravascular imaging.

4 Conclusion

We have presented a miniaturized integrated probe combining US and PA. The probe was built by integrating a ring-shaped US transducer with a coaxial optical fiber and a micromirror. By introducing the fiber delivery system to the US-based catheter, the sample could be illuminated internally which revealed its clinical potential. The micromirror deflected coaxial sound and light beam at the same angle making the probe simple and easy to align. Overlapping the sound and light beam along the whole transmitting path could potentially improve the probe's working distance. In the phantom study, the performance of the probe was evaluated and the complementary IVUS/IVPA images emphasized the synergy of the combined US and PA system. The coaxially designed probe provided coregistered IVUS and IVPA images of a normal rabbit aorta which also demonstrated the imaging ability of this dual-modality system.

Acknowledgments

We would like to thank Ms. Hongrui Li for preparing the tissue. This work is based on the research supported by the NIH (Grant Nos. EB-00293, EB-10090, RR-01192, and P41-EB2182) and the U.S. Air Force Office of Scientific Research, Medical Free-Electron Laser Program Grant No. FA9550-08-1-0384. Wei Wei is supported in part by the China Scholarship Council (CSC) and works as a joint Ph.D. student at the Beckman Laser Institute and Medical Clinic, University of California, Irvine.

References

1. "National Heart and Blood Institute," http://www.nhlbi.nih.gov/health/dci/index.html.
2. G. Pasterkamp, E. Falk, H. Woutman, and C. Borst, "Techniques characterizing the coronary atherosclerotic plaque: Influence on clinical decision making," *J. Am. Coll. Cardiol.* **36**, 13–21 (2000).
3. A. M. Shah, A. H. Feldman, D. L. George, and D. Edmundowicz, "Role of electron beam computed tomography in detecting and assessing coronary artery disease," *Hosp. Physician* **43**(3), 11–18 (2007).
4. G. J. Tearney, I. K. Jang, and B. E. Bouma, "Optical coherence tomography for imaging the vulnerable plaque," *J. Biomed. Opt.* **11**(2), 021002 (2006).
5. F. S. Foster, C. J. Pavlin, K. A. Harasiewicz, D. A. Christopher, and D. H. Turnbull, "Advances in ultrasound biomicroscopy," *Ultrasound Med. Biol.* **26**(1), 1–27 (2000).
6. T. Sawada, J. Shite, H. M. Garcia-Garcia, T. Shinke, S. Watanabe, H. Otake, D. Matsumoto, Y. Tanino, D. Ogasawara, H. Kawamori, H. Kato, N. Miyoshi, M. Yokoyama, P. W. Serruys, and K. Hirata, "Feasibility of combined use of intravascular ultrasound radiofrequency data analysis and optical coherence tomography for detecting thin-cap fibroatheroma," *Eur. Heart J.* **29**, 1136–1146 (2008).
7. L. V. Wang, Ed., *Photoacoustic Imaging and Spectroscopy*, Taylor & Francis/CRC Press Boca Raton, FL (2009).
8. A. A. Oraevsky and A. A. Karabutov, in *Biomedical Photonics Handbook*, T. Vo-Dinh, Ed., Vol. PM125, Chapter 34, CRC Press Boca Raton, FL (2003).
9. K. Maslov, G. Stoica, and L. V. Wang, "In vivo dark-field reflection-mode photoacoustic microscopy," *Opt. Lett.* **30**(6), 625–627 (2005).
10. H. F. Zhang, K. Maslov, G. Stoica, and L. V. Wang, "Functional photoacoustic microscopy for high-resolution and noninvasive in vivo imaging," *Nat. Biotechnol.* **24**, 848–851 (2006).
11. J. M. Yang, K. Maslov, H. C. Yang, Q. F. Zhou, K. K. Shung, and L. V. Wang, "Photoacoustic endoscopy," *Opt. Lett.* **34**(10), 1591–1593 (2009).
12. S. Sethuraman, J. H. Amirian, S. H. Litovsky, R. Smalling, and S. Y. Emelianov, "Ex vivo characterization of atherosclerosis using intravascular photoacoustic imaging," *Opt. Express* **15**, 16657–16666 (2007).
13. B. Wang, J. L. Su, J. Amirian, S. H. Litovsky, R. Smalling, and S. Y. Emelianov, "Detection of lipid in atherosclerotic vessels using ultrasound-guided spectroscopic intravascular photoacoustic imaging," *Opt. Express* **18**, 4889–4897 (2010).
14. W. Wei, X. Li, Q. F. Zhou, K. K. Shung, and Z. P. Chen, "Development of a combined ultrasound and photoacoustic endoscopic probe," *Proc. SPIE* **7893**, 789317 (2011).
15. S. Sethuraman, S. R. Aglyamov, J. H. Amirian, R. W. Smalling, and S. Y. Emelianov, "Intravascular photoacoustic imaging using an IVUS

imaging catheter," *IEEE Trans. Ultrason. Ferroelectr. Freq. Control* **54**(5), 978–986 (2007).
16. B.-Y. Hsieh, S.-L. Chen, T. Ling, L. J. Guo, and P.-C. Li, "An integrated intravascular ultrasound and photoacoustic imaging scan head," *Opt. Lett.* **35**(17), 2892–2894 (2010).
17. A. B. Karpiouk, B. Wang, and S. Y. Emelianov, "Development of a catheter for combined intravascular ultrasound and photoacoustic imaging," *Rev. Sci. Instrum.* **81**, 014901 (2010).
18. K. Jansen, A. F. W. van der Steen, H. M. M. van Beusekom, J. W. Oosterhuis, and G. van Soest, "Intravascular photoacoustic imaging of human coronary atherosclerosis," *Opt. Lett.* **36**(5), 597–599 (2011).
19. Laser Institute of America, *American National Standard for the Safe Use of Lasers*, ANSI Z136.1–2000, American National Standards Institute, Inc. (2000).
20. J. T. Dodge, Jr., B. G. Brown, E. L. Bolson, and H. T. Dodge, "Lumen diameter of normal human coronary arteries. Influence of age, sex, anatomic variation, and left ventricular hypertrophy or dilation," *Circulation* **86**, 232–246 (1992).
21. A. Iannuzzi, M. D. Michele, S. Panico, E. Celentano, R. Tang, M. G. Bond, L. Sacchetti, F. Zarrilli, R. Galasso, M. Mercuri, and P. Rubba, "Radical-Trapping Activity, Blood Pressure, and Carotid Enlargement in Women," *Hypertension* **41**, 289–296 (2003).
22. R. S. C. Cobbold, *Foundations of Biomedical Ultrasound*, pp. 51–180, Oxford University Press, New York (2007).
23. X. Li, J. C. Yin, C. H. Hu, Q. F. Zhou, K. K. Shung, and Z. P. Chen, "High-resolution coregistered intravascular imaging with integrated ultrasound and optical coherence tomography probe," *Appl. Phys. Lett.* **97**, 133702 (2010).
24. "Optical Properties Spectra," http://omlc.ogi.edu/spectra/.
25. K. C. Hoang, A. Edris, J. P. Su, D. S. Mukai, S. Mahon, A. D. Petrov, M. Kern, C. Ashan, Z. P. Chen, B. J. Tromberg, J. Narula, and M. Brenner, "Use of an oxygen-carrying blood substitute to improve intravascular optical coherence tomography imaging," *J. Biomed. Opt.* **14**(3), 034028 (2009).
26. B. Wang, J. L. Su, A. B. Karpiouk, K. V. Sokolov, R. W. Smalling, and S. Y. Emelianov, "Intravascular Photoacoustic Imaging," *IEEE J. Sel. Top. Quant. Electron.* **16**(3), 588–599 (2010).
27. T. J. Allen, A. Hall, A. Dhillon, J. S. Owen, and P. C. Beard, "Photoacoustic imaging of lipid rich plaques in human aorta," *Proc. SPIE* **7564**, 75640C (2010).
28. I. M. Graf, J. Su, D. Yeager, J. Amirian, R. Smalling, and S. Emelianov, "Methodical study on plaque characterization using integrated vascular ultrasound, strain and spectroscopic photoacoustic imaging," *Proc. SPIE* **7899**, 789902 (2011).
29. H. W. Wang, N. Chai, P. Wang, S. Hu, W. Dou, D. Umulis, L. V. Wang, M. Sturek, R. Lucht, and J. X. Cheng, "Label-free bond-selective imaging by listening to vibrationally excited molecules," *Phys. Rev. Lett.* **106**(1), 238106 (2011).
30. J. C. Yin, H. C. Yang, X. Li, J. Zhang, Q. F. Zhou, C. H. Hu, K. K. Shung, and Z. P. Chen, "Integrated intravascular optical coherence tomography ultrasound imaging system," *J. Biomed. Opt.* **15**(1), 010512 (2010).